ISSN 1027-5495. Functional Materials, 30, No.2 (2023), p. 282-289.
doi:https://doi.org/10.15407/fm30.02.282

Growth of Fe-BTC particles beneath stearic acid Langmuir monolayers and research on its adsorption of methyl orange

Yuan-Sheng Ding, Fei Lu

School of Chemistry and Pharmaceutical Engineering, Jilin Institute of Chemical Technology, 132022 Jilin, P.R.China

Received March 23, 2023

Langmuir monolayers of stearic acid (SA) were used as a template to induce the nucleation and growth of Fe-BTC microparticles. X-ray diffraction (XRD) patterns, Fourier transform infrared spectroscopy (FTIR), BET and microscopy techniques were employed to investigate the particles. In the absence of the template, the Fe-BTC particles show a bulky morphology, while round-shaped Fe-BTC is nucleated beneath a Langmuir monolayer. The Fe-BTC material has been found to have excellent adsorption properties for the organic dye methyl orange in aqueous solutions, exhibiting both high adsorption capacity and rate. Adsorption capacity of Fe-BTC for Methyl Orange(MO) was retained high and stable in a wide range of pH values from 2 to 9. The adsorption capacity of Fe-BTC for MO is described by a pseudo-second-order model, implying that chemisorption is responsible for the process. The adsorption data were analyzed and found to be in line with the Langmuir isotherm model, indicating the monolayer adsorption.

Keywords: Langmuir monolayer, Fe-BTC, bionic mineralization, adsorption; methyl orange.

Зростання частинок Fe-BTC на моношарах Ленгмюра стеаринової кислоти та адсорбційні властивості метил оранжу. *Yuan-Sheng Ding, Fei Lu*

Ленгмюрівські моношари стеаринової кислоти (SA) використовували як матрицю для індукції зародження та росту мікрочастинок Fe-BTC. Для дослідження частинок використовували рентгенограми (XRD), інфрачервону спектроскопію з перетворенням Фур'є (FTIR), БЕТ та мікроскопію. За відсутності матриці частинки Fe-BTC демонструють об'ємну морфологію, тоді як Fe-BTC округлої форми зароджується на моношарі Ленгмюра. Було виявлено, що матеріал Fe-BTC має чудові адсорбційні властивості для органічного барвника метилового оранжевого у водних розчинах, показуючи як високу адсорбційну здатність, так і швидкість. Адсорбційна здатність Fe-BTC для метилового апельсина (MO) залишалася високою та стабільною в широкому діапазоні значень pH від 2 до 9. Адсорбційна здатність Fe-BTC для MO описується моделлю псевдодругого порядку, що передбачає що за процес відповідає хемосорбція. Дані адсорбції були проаналізовані та виявили, що вони відповідають моделі ізотерми Ленгмюра, що вказує на моношарову адсорбцію.

1. Introduction

Synthetic dyes are widely used in plastics, textiles, rubber, cosmetics, food processing, medicine, and other industries that are the most crucial water contamination sources [1, 2]. The discharge of these colored dyes into the water can affect the photosynthesis of aquatic organisms with mutagenic properties [3]. Moreover, these dyes can also cause harm to the human central nervous system, reproductive system, kidney, etc [4, 5]. Some species are even carcinogenic [6]; therefore, the dye-containing

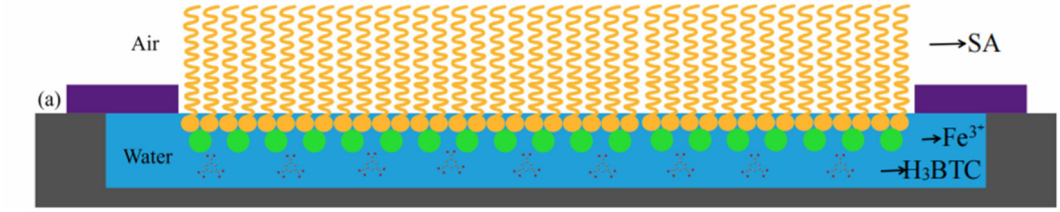

Fig.1. Schematic diagram of the biomineralization experimental set-up.

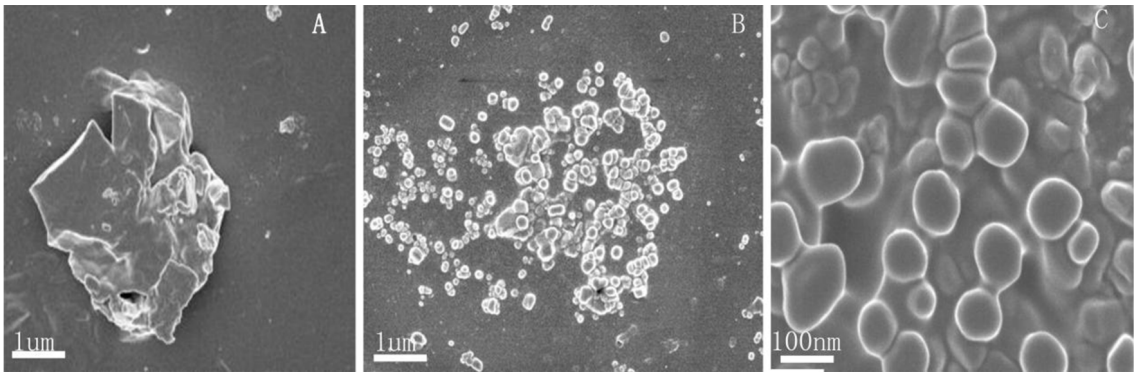

Fig.2. SEM images of Fe-BTC grown (A) in aqueous solution, (B) on a Langmuir monolayer of stearic acid, (C) Enlarge image of (b).

wastewater should be treated somewhat before being discharged.

Metal-organic frameworks (MOFs) refer to coordination compounds [7] formed by organic ligands and metal ions or metal clusters through coordination bonds. MOFs materials are characterized by a lot of pores, large specific surface area, diverse structures, and functional diversity. They have been used in gas storage, catalysis, chemical separation, and so on [8]. In recent years, dye absorbents from MOFs have attracted much attention [9]. Iron-based MOFs are excellent absorbents because the iron matrix is inexpensive. As one of the few commercial MOFs materials, Fe-BTC is at the focus of our research. Fe-BTC is a 1,3,5-Benzenetricarboxylic acid (H3BTC) linker-based MOFs based on Fe(III) with some degree of the missing ligand [10]. Amorphous Fe-BTC materials are usually prepared by the sol-gel method, followed by drying or annealing [11]. In this process, the use of strong acids, high temperatures, or the use of high-boiling organic solvents is unavoidable. However, some research groups have adopted the "room temperature transformation" strategy to prepare Fe-BTC in aqueous or ethanol solutions at room temperature without the further post-processing [12, 13]. However, the morphology of the materials formed at room temperature is mostly irregular.

The ability of biological systems to control inorganic crystal structure, phase, orientation, and nanostructure morphology is called biomineralization. Biomineralization is considered as one of the biomimetic pathways to prepare nanostructured materials, which has many advantages over other solid-state and wet-chemical methods [14]. Professor Mann of Bristol University has pointed out that biological minerals are usually synthesized on the surface of organic templates such as the biomacromolecule framework, lipid membranes or cell walls [15]. Langmuir monolayers have a semidiphospholipid membrane structure, which is similar to the structural morphology of biofilm. Many inorganic and organic materials have been prepared to use Langmuir monolayers as biomineralization templates [16–17].

In this article, circular Fe-BTC particles were well formed using biomineralization simulation methods using a Langmuir SA monolayer. The biomimetic mineralization process was inspected by a metallography microscope every hour. The adsorption properties of methyl orange were studied, and the effects of the initial concentration of methyl orange, contact time, adsorbent dosage and pH on the adsorption ability were discussed. In addition, the isothermal adsorption and adsorption kinetics of adsorbing methyl orange with Fe-BTC were studied to understand its adsorption mechanism.

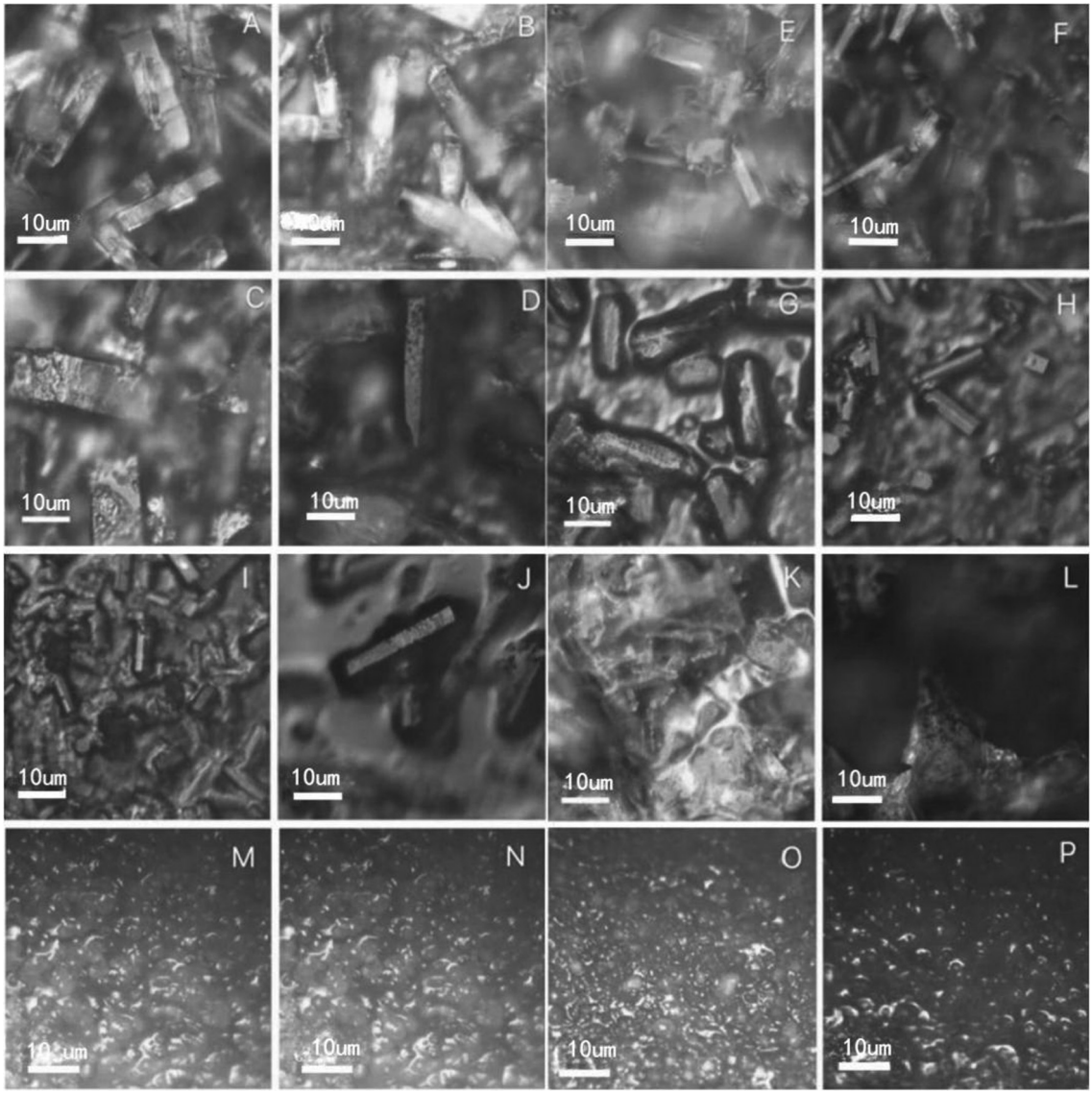

Fig.3. Metallographic images of Fe-BTC on an SA monolayer after growth for A-2h, B-4h, C-6h, D-8h, E-9h, F-10h, G-11h, H-12h, I-12h, J-13h, K-14h, L-16h, M-18h, N-20h, O-22h, P-24h).

2. Experimental

Chemicals.

Stearic acid, $FeCl_3$, and H_3BTC were obtained from Fluka Chemical Co. and used without further purification. The chloroform and acetone were of A.R. grade and were purchased from the Shanghai Chemical Reagents Co.

Preparation of Fe-BTC particles.

Triple distilled deionized water (Ultrapure Millipore water, 18.2 M·Ω) containing 10 mM $FeCl_3$ and 50 mM H_3BTC is used as a subphase. The 10^{-3} mol chloroform SA solution was spread on the subphase with a microsampler. The Chloroform was allowed to evaporate for at least 30 min before compression was started. The Langmuir monolayer was slowly compressed at 15 mNm^{-1} and maintained at that pressure during the material growth. The crystals were aspirated from the surface of the subphase using a syringe after different mineralization times. All the experiments were performed at room temperature. The schematic diagram of the biomineralization experimental set-up is shown in Fig. 1.

Characterization.

X-ray diffraction (XRD) patterns were recorded with a D/Max-RA X-ray diffractometer using CuKα radiation. The morphology of obtained crystals was observed by a JSM-5600 scanning electron microscope (SEM) and a metallographic microscope. The

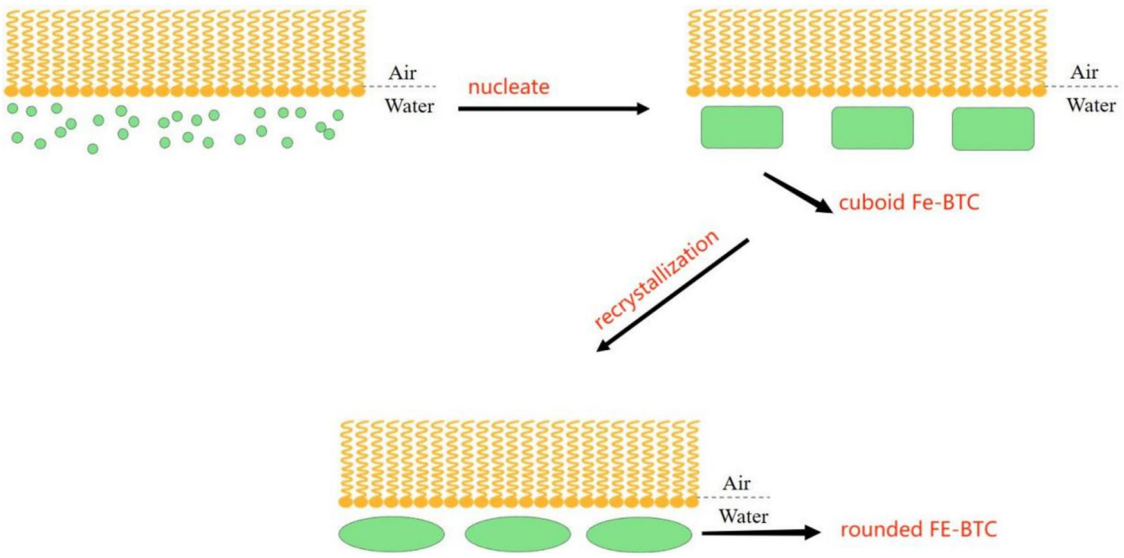

Fig.4. Scheme of growth process of Fe-BTC particles with the induction of a SA Langmuir monolayer.

FTIR spectrum was measured by a Perkin Elmer FTIR1600 spectrometer.

Adsorption experiments.

The adsorption ability of Fe-BTC for MO was evaluated as follows: different amounts of adsorbents were placed in 10 ml of water, then a dye was added at a certain concentration at room temperature. After centrifugation and separation, the dye concentration in the supernatant was settled, and the adsorption capacity (q_t) was calculated according to Equation (1):

$$q_t = (c_0 - c_t) \cdot V/m, \quad (1)$$

where c_0 is the starting concentration of dye (mg/L); c_t is the concentration of the dye after some time adsorption (mg/L); V is the volume of the dye (mL); m is the mass of the adsorbent (mg). The adsorption time was changed from 55 to 540 min, and the curve of adsorption capacity with time was measured when the 9 mg Fe-BTC was put in 10 mL MO solutions (25 mg/L). The pH of the dye solution was adjusted from 2 to 12, and the curve of adsorption capacity with pH was measured, when the 9 mg Fe-BTC was placed in 10 mL MO solutions (25 mg/L). Cyclic adsorption of Fe-BTC was also measured under the same conditions.

3. Results and discussion

Fig. 2A shows an example of Fe-BTC particles grown from the neutral solution. The sample morphology is irregular, and its rough particle surface does not display angular particle morphology. In contrast, the Fe-BTC particles induced by the SA template (Fig. 2B) have a circular morphology, indicating that the SA Langmuir monolayer can well regulate the growth of Fe-BTC particles.

Fig. 3 shows the optical microscopic images of the particle morphology at different mineralization times. At the initial stage of mineralization, the morphology of the particle grains is rectangular, and the particles are micrometer in size. With an increase in the time of mineralization, the size of the cuboid particles gradually decreased. After 16 hours, the cuboid particles disappeared, and round particles appeared. From 18 hours, the rounded morphology becomes the dominant morphology. The above experimental phenomena indicate that the growing Fe-BTC particles undergo nucleation, dissolution, and recrystallization upon induction of a Langmuir SA monolayer. The scheme for the process is shown in Fig. 4.

Fig. 5 shows a FTIR spectrum of the obtained Fe-BTC sample with a growth time of 24 hours. The absorption peak at 480 cm^{-1} is the stretching vibration peak of the FeO octahedron. The peaks at 713, 760, and 1030 cm^{-1} belong to the out-of-plane bending vibration of C–H on the benzene ring. The absorption peak at 1109 cm^{-1} corresponds to the stretching vibration of C–O on the carboxyl group. The strong peak at 1380 cm^{-1} corresponds to the overlap of the Fe–OH vibration and COO^- stretching vibration under the influence of coordinated Fe in the structure [18]. The peak at

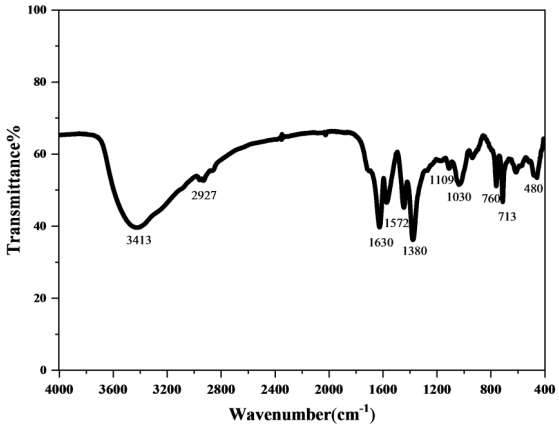

Fig.5. FT-IR spectrum of obtained Fe-BTC particles.

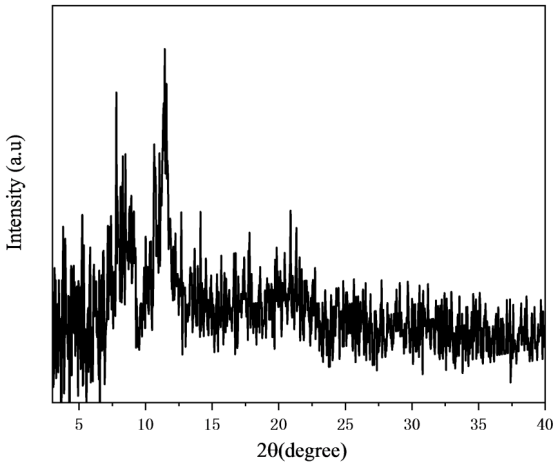

Fig.6. XRD pattern of obtained Fe-BTC particles.

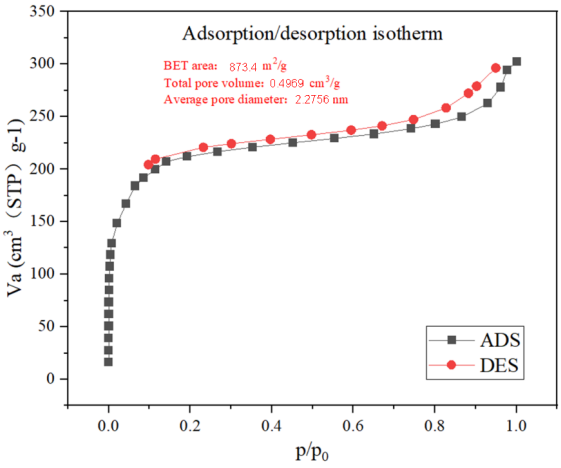

Fig.7. N_2 adsorption-desorption isotherms of obtained Fe-BTC particles.

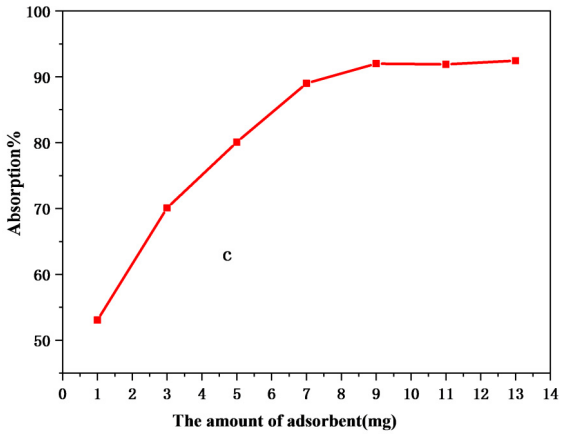

Fig. 8. Effect of the amount of Fe-BTC on MO dye adsorption percentage.

1572 cm^{-1} corresponds to the asymmetric stretching vibration of -COO^-, and the stronger peak at 1630 cm^{-1} corresponds to C=O on the triphenyl acid ligand. The absorption peak at 2927 cm^{-1} is the stretching vibration peak of C–H of the benzene ring, and the absorption peak at 3413 cm^{-1} is the stretching vibration peak of H_2O molecule in MOFs and carboxyl-OH on the ligand of triphenylacid [19]. The spectrum shows that the structural composition of the sample is similar to the spectrum of Fe-BTC prepared in the previous studies.

The XRD pattern can generally reflect the microstructure of porous materials. Unlike MIL-100(Fe), the peak positions of Fe-BTC are fuzzy and disordered (Fig. 6), which indicates that the synthesized Fe-BTC is an amorphous material with a low spatial structure order. The experimental results on Fe-BTC are consistent with the previous literature reports [20]: the XRD pattern shows that Fe-BTC has a spatially distorted structure of MIL-100(Fe) to a certain extent.

In Fig. 7, the nitrogen adsorption-desorption isotherm of Fe-BTC at 77 K is shown. This isotherm is a typical type I isotherm, and a sharp increase at a relatively low pressure indicates that the Fe-BTC particles have a microporous structure with a pore size of 2.28 nm. The micropore volume of Fe-BTC particles is approximately 0.50 cm^3/g, and the BET specific surface area is 873.3 m^2/g.

From Fig. 8, it can be seen that the amount of Fe-BTC has a significant effect on the adsorption efficiency of methyl orange in the solution. The Fe-BTC dosage affects the adsorption efficiency of methyl orange in solution, under the condition of a fixed initial mass concentration of methyl orange and adsorption time. With the

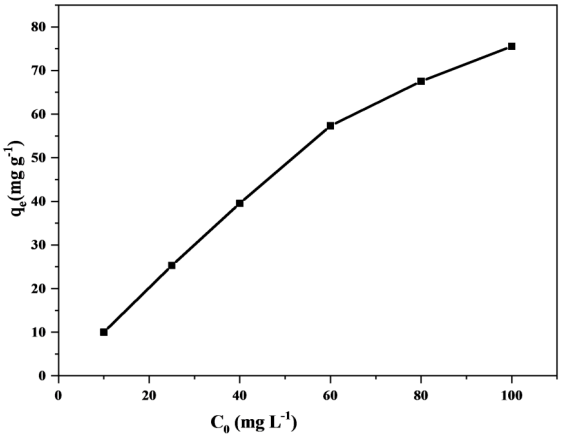

Fig. 9. Adsorption amounts in methyl orange solutions of different mass concentrations.

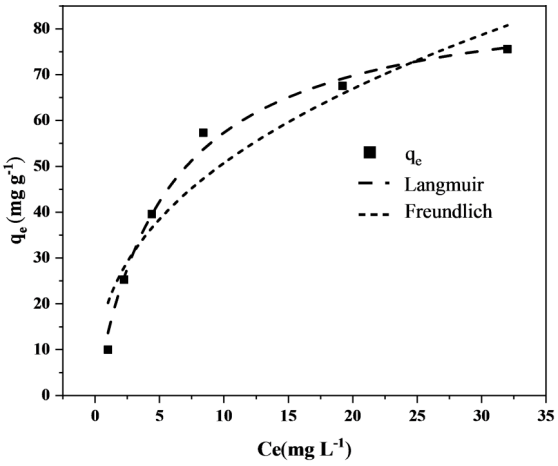

Fig. 10. Adsorption isotherms of MO dye on the Fe-BTC particles.

amount of Fe-BTC equal to 1 mg, the number of adsorption centers existing on the surface is not enough to carry out complete adsorption separation of adsorbed dyes in solution, and the adsorption efficiency is only 53.06 %. With an increase in the dosage of adsorbent, MO in the solution can be largely adsorbed and removed; and at a dosage of 9 mg Fe-BTC, the adsorption rate of MO reaches 92.06 %. After that, the adsorption rate of the adsorbent was stable. It indicates that the dosage of 9 mg can provide complete adsorption and removal of ions from solution under current experimental conditions. However, the ion adsorption and separation efficiency cannot achieve 100 % due to a phenomenon of MO molecular desorption from the surface of Fe-BTC in the course of the adsorption process. Consequently, we choose the dose of 9 mg as the optimal parameter.

The equilibrium adsorption capacity Q_e (mg/g) of prepared Fe-BTC with respect to methyl orange solutions with different initial mass concentrations of 10, 25, 40, 60, 80 and 100 mg/L for 24 h was investigated (Fig. 9). It can be seen from Fig. 9 that the equilibrium adsorption capacity to methyl orange increases with an increase in the mass concentration of methyl orange, and the slope of the curve is larger when the mass concentration of methyl orange is low. The slope gradually decreases, indicating that the adsorption gradually reaches saturation.

The adsorption of methyl orange in different mass concentrations was analyzed using two isotherm adsorption models: Langmuir model and Freundlich model. The Langmuir model gives the highest correlation coefficient, as shown in Table 1 and Fig. 10. This suggests that the adsorption of methyl orange on Fe-BTC occurs in the form of a monolayer, as assumed by the model. The separation factor R_L is used to determine if the adsorbent has preferential or non-preferential dye adsorption. It is expressed as: $R_L = 1/(1 + K_L \cdot C_0)$. The calculated R_L falls between 0 and 1, indicating that the adsorption of dye methyl orange on Fe-BTC is feasible.

We also examined the effect of the contact time on the adsorption process of methyl orange by Fe-BTC at different temperatures under the condition of pH 7.0 in the solution system. As can be seen from Fig. 11, as the reaction time increased, adsorption increased first rapidly and then slowly. When the contact time reached 150 min, the adsorption of methyl orange on Fe-BTC basically reached equilibrium. At the beginning of the reaction, there are a great number of adsorption sites on the surface of the adsorbent material, which can react with the methyl orange in the solution, so that methyl orange is adsorbed

Table 1. Isotherm model constants for adsorption of MO dye on the Fe-BTC particles

Langmuir model			Freundlich model		
q_m, mg g^{-1}	K_L, L·mg^{-1}	R^2	K_F	n	R^2
0.018	0.1809	0.9966	20.2136	2.501	0.9293

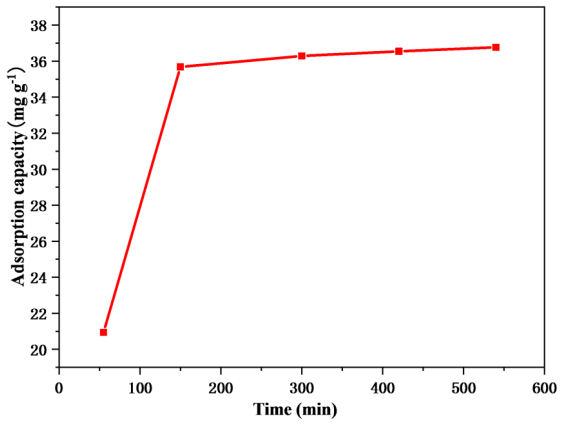

Fig. 11. Contact time on adsorption percentage of MO dye on the Fe-BTC particles.

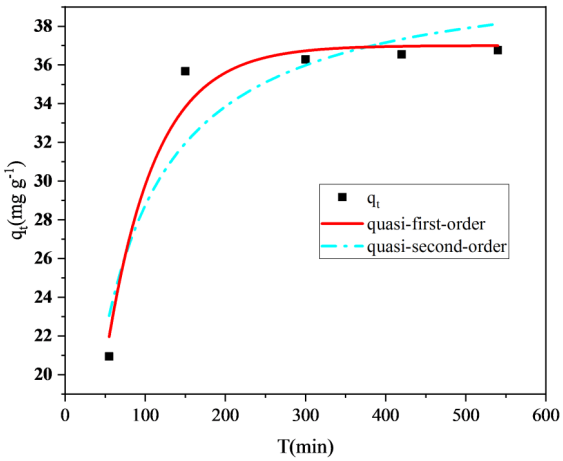

Fig. 12. Adsorption kinetics, quasi-first-order and quasi-second-order kinetic models.

quickly. With the progress of the reaction, the adsorption sites on the surface of the adsorbent material are occupied by methyl orange, and MO loaded into adsorption sites prevents diffusion of MOs to the adsorbent in solution, so the adsorption process reaches equilibrium.

The results of fitting the adsorption kinetic curves are shown in Fig. 12 and Table 2. Combined with the fitting-related parameters in Table 2, the equilibrium adsorption capacity qcal obtained using the quasi-first-order kinetic model is far different from the experimental equilibrium adsorption capacity qe. The equilibrium adsorption amount obtained by the quasi-second-order kinetic model is close to the qe, and the linear correlation coefficient R^2 is close to 1. Thus, in the process of MO adsorption on the Fe-BTC conforms, the chemical interaction predominates [21].

Fig. 13 shows the effect of pH value on the adsorption of methyl orange. It can be seen that below pH 9, the amount of adsorbed methyl orange material does not change much. When the pH value is higher than 9, the adsorption ratio is greatly reduced due to the destruction of the Fe-BTC structures under highly alkaline conditions.

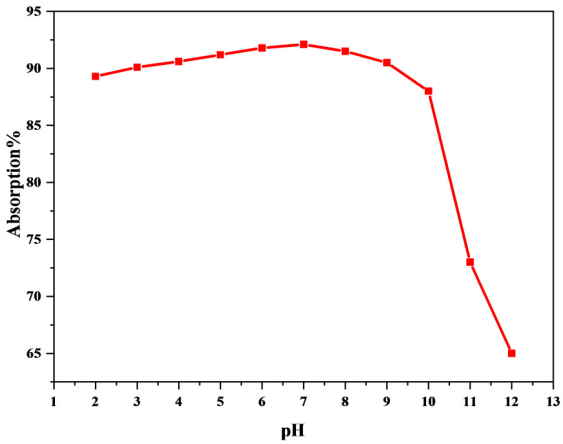

Fig. 13. Effect of the pH on adsorption percentage of MO dye on the Fe-BTC particles.

The pH value of most aqueous media is typically below 9, so for most wastewater treatment processes, the use of Fe-BTC can provide a better methyl orange adsorption effect without changing the pH value of the system. Therefore, compared with other adsorption materials, Fe-BTC has a great advantage in the application of methyl orange adsorption. The surface of the Fe-BTC adsorption material is positively charged when

Table 2. Kinetic parameters of kinetic models for adsorption of MO dye on the Fe-BTC particles

c, mg/g	q_{exp}, mg/g	Quasi-first-order kinetic model			Quasi-second-order kinetic model		
		k_1(min)	q_{cal}	R^2	k_2 (g mg^{-1}min^{-1})	q_{cal}	R^2
9	37.04	0.018	5.3	0.985	0.001	39.05	0.995

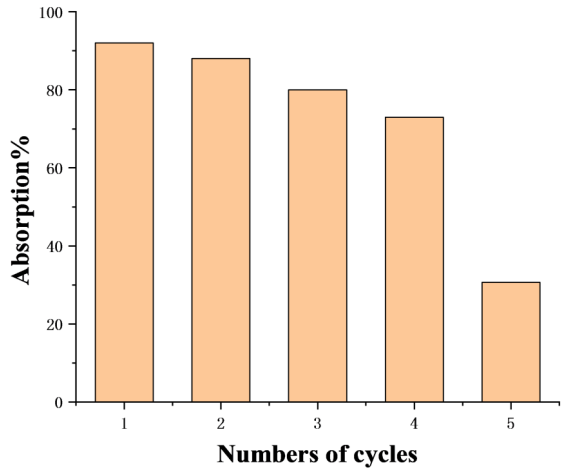

Fig. 14. Adsorption percentage of MO dye on the Fe-BTC particles with various numbers of cycles.

the pH is lower than 9 [22], while methyl orange is an acidic dye containing a sulfonate anion (-SO_3Na), whose dissociation constant p_{Ka} is 3.4. When the pH value of the solution is greater than its dissociation constant, methyl orange mainly exists in the form of an anion (MO-) [22]. Hence, when the pH is between 3.4 and 9, there is a strong electrostatic interaction between MO and Fe-BTC. When the pH is below 3.5, the π–π stacking interaction between the benzene rings and hydrogen in the MOF organic linker and the MO molecule, which determines the adsorption ratio, is still at a high level.

The results of the reusability tests in Fig. 14 show, that the adsorption amount of Fe-BTC gradually decreases as the adsorption time increases. After 5 cycles, the rate of Fe-BTC to absorb methyl orange dropped to 30.64 %. The reason may be that the chemical desorption process is not accomplished enough; as a result, some dye molecules remain in the Fe-BTC pore structure, reducing the specific surface area and the number of adsorption sites of Fe-BTC in the cyclic adsorption, which will in turn reduce the adsorption effect of Fe-BTC on the methyl orange.

4. Conclusion

Circular Fe-BTC particles were nucleated on a Langmuir SA monolayer by simple simulated biomineralization methods at room temperature. The microscopy results show that the growth of Fe-BTC occurs by the nucleation-dissolution-recrystallization mechanism under the action of the Langmuir SA monolayer. Fe-BTC prepared by the method can effectively remove methyl orange in a large pH range. The adsorption of methyl orange by Fe-BTC is in good agreement with both the quasi-second order adsorption kinetic model and the Langmuir isotherm model. The results show that the process of methyl orange adsorption by the Fe-BTC adsorbent belongs to monolayer adsorption, chemisorption prevails in the adsorption process.

Acknowledgments. This research was supported by the Jilin Province Education Department project (No. 202350253)

References

1. C.Y.Tang, P.Yu, L.S.Tang et al., *Ecotoxicol. Environ. Saf.*, **165**, 299 (2018).
2. Y.C.Yu, Z.J.Hu, Y.L.Zhang, H.W.Gao, *RSC Adv.*, **6**, 18577 (2016).
3. N.B.Turan, H.S.Erkan, F.Ilhan, G.O.Engin, *Water Environ. Res.*, **94**, e1683.1 (2022).
4. T.Q.Liu, C.O.Aniagor, M.I.Ejimofor et al., *J. Ind. Eng. Chem.*, **117**, 21 (2023).
5. D.Mondal, S.Roy, S.Bardhan et al., *S. Das. Dalton. Trans.*, **51**, 451 (2022).
6. M.D.M.Darder, M.Bedoya, L.A.Serrano et al., *Sens. Actuators B. Chem.*, **353**, 131099 (2022).
7. B.Panella, M.Hirscher, H.Putter, U.Muller, *Adv. Funct. Mater.*, **16**, 520 (2006).
8. M.U.Nisa, Y.Chen, X.Li, Z.Li, *J. Taiwan. Inst. Chem. Eng.*, **51**, 10744 (2020).
9. M.Li, G.Ren, W.Yang et al., *Chem. Commun.*, **57**, 1340 (2021).
10. A.Zukal, M.Opanasenko, M.Rube et al., *Catal Today*, **2015**, 24369 (250).
11. F.Dorosti, A.Alizadehdakhel, *Saf. Environ. Prot.*, **136**, 119 (2018).
12. G.R.Delpiano, D.Tocco, L.Medda et al., *J. Mol. Sci.*, **22**, 788 (2021).
13. E.Garcia, Rojas Medina, Ricardo Lopez, Lozano, & M.May et al., *Materials*, **7**, 8037 (2014).
14. I.Segovia-Campo, A.Martignier, M.Filel et al., *Micro. Biol.*, **24**, 537 (2022).
15. A.W.Williams, D.S.Jackson, A.J.Grillo et al., *Small*, **6**, 1191 (2010).
16. M.Mahato, P.Pal, B.Tah et al., *Mater. Chem. Phys.*, **137**, 665 (2013).
17. Z.H.Xue, B.B.Hu, X.L.Jia et al., *Mater. Chem. Phys.*, **114**, 47 (2009).
18. S.Bhattacharjee, *Indian J. Chem.*, **57**, 778 (2018).
19. F.Dorosti, A.Alizadehdakhel, *Chem. Eng. Res. Des.*, **136**, 119 (2018).
20. A.Yuan, Y.Lu, X.Zhang et al., *J. Mater. Chem. B*, **8**, 9295 (2020).
21. H.Liang, C.Zou, *Can. J. Chem. Eng.*, **97**, 1894 (2019).
20. A.Karami, R.Shomal, R.Sabouni et al., *Energies*, **15**, 4642 (2022).